

Synthesis, characterization and photoluminescence properties of $Y_2O_3:Eu^{3+}$ phosphor

Shah Abdul Haseeb¹ and Sudeshna Ray¹

¹Department of Physical Science, Faculty of Science, Rabindranath Tagore University, Bhopal 464551, M. P., India

Abstract -

Synthesis of nanocrystalline $Y_2O_3:Eu^{3+}$ phosphor by complex based precursor solution method, using triethanolamine (TEA) as complexing agent, has been described. The synthesis of corresponding bulk sample has also been reported. The samples have been characterized through x-ray diffraction (XRD) and transmission electron microscopy (TEM) measurements. The intensity of the nanocrystalline phosphor is found to be maximum when the concentration of Eu^{3+} is 4 at wt% with respect to Y^{3+} , after which, 'concentration quenching' starts dominating.

Key Words - triethanolamine (TEA), Nanocrystalline, Phosphor

1. Introduction

Yttrium oxide (Y_2O_3) doped with trivalent europium ion (Eu^{3+}) is one of the main red-emitting phosphors [1-5]. The unique optical property of this material is based on the *f* and d electrons of europium ions. To enhance the brightness and resolution of displays in devices in the present nanotechnology regime, it is important to develop phosphors with controlled morphology and small particle size (nanoparticles). The potential applications of this low dimensional material in fabrication of modern micro/nano devices require an understanding of their fundamental optical properties in detail. For example, permanent laser-induced gratings have been fabricated using crossed write beams in resonance with the ${}^7F_0 \rightarrow {}^5D_2$ absorption transition of Eu^{3+} doped phosphors [6]. Thus, the origin and behavior of the strongest ${}^7F_0 \rightarrow {}^5D_2$ transition spectrum from Eu^{3+} needs to be investigated because of its importance in design in Glaser devices.

Over the last couple of decades, a considerable amount of work on the spectral properties of bulk $Y_2O_3:Eu^{3+}$ has been reported in the literature [7-15]. Additionally, we find several articles on nanoparticles of this material (as described in Chapter 1), though, the detailed study of their optical properties is, as far as we are aware, incomplete. Apart from a

detail study on the emission characteristics, in this chapter we also present the estimation of the crystal field parameter and the equilibrium thermal energy of this nanocrystalline phosphor. The knowledge of these two parameters is very crucial for the application of the phosphor.

We discuss the synthesis of nanocrystalline and bulk $Y_2O_3:Eu^{3+}$ phosphors; covers the characterization of the phosphors by x-ray diffraction (XRD) and transmission electron microscopy (TEM) measurements. Photoluminescence (PL) properties of the nanocrystalline and bulk phosphors have been discussed.

1.2 Synthesis

1.1.1 Synthesis of nanocrystalline sample

The nanomaterial has been prepared by complex based precursor solution method using triethanolamine (TEA) as complexing agent [16]. Solid powder of europium oxide (Eu_2O_3) and yttrium oxide (Y_2O_3) (both from ALDRICH) are boiled with concentrated nitric acid in water bath in order to get clear solutions of europium nitrate [$Eu(NO_3)_3$] and yttrium nitrate [$Y(NO_3)_3$], respectively. $Eu(NO_3)_3$ and $Y(NO_3)_3$ solutions are taken in different stoichiometric ratios in order to vary the Eu^{3+} concentration by 1–7 at. wt. % with respect to Y^{3+} . Then, the requisite amount of TEA was mixed with the nitrate solution to maintain the total metal ion to TEA mole ratio at 1:4. In the beginning, TEA formed a precipitate (because of the formation of metal hydroxides) with metal ions. This precipitate was dissolved and a clear solution was obtained by adding a certain amount of HNO_3 , maintaining the pH at 3 – 4. The clear solution of TEA-complexed metal nitrate was evaporated on a hot plate at $180\text{ }^\circ\text{C}$ – $200\text{ }^\circ\text{C}$ with constant stirring. Continuous heating of the solution led to foaming and puffing. During evaporation, the nitrate ions provide an in-situ oxidizing environment for TEA, which partially converts the hydroxyl groups of TEA into carboxylic acids. When complete dehydration occurred, the nitrates themselves decomposed, with the evolution of brown fumes of nitrogen dioxide, leaving behind a voluminous, organic-based, black, fluffy powder, i.e., the precursor powder. The precursor mass was then calcined at $500\text{ }^\circ\text{C}$ for 2 hrs. and then annealed at $900\text{ }^\circ\text{C}$ for 2 hrs. to get the required nanocrystalline sample.

1.1.2 Synthesis of bulk sample

The Calcined sample was sintered at 1400 °C for 2 hr in order to get the bulk sample. When the concentration of Eu^{3+} is 4 at. wt. %, the emission intensity of the nanocrystalline phosphor is found to be maximum (will be discussed in Section 2.4). For this reason, in the rest of chapter, $\text{Y}_2\text{O}_3:\text{Eu}^{3+}$ (with 4 at. wt. % of Eu^{3+}) samples, both nanocrystalline and bulk, have been taken as reference samples for characterization.

1.1.3 Mechanism of the synthetic procedure

The preparation procedure involved the evaporation of aqueous precursor solutions, which were composed of stoichiometric amounts of the desired metal ions, complexed with TEA. TEA is an efficient chelating agent that has good coordination properties with the metal ions. One to two moles of TEA per mole of the total metal ions are stoichiometrically required for formation of stable complexes with metal ions. However, TEA in the precursor solution has always been maintained to be in excess of the required stoichiometry. During evaporation of the precursor solution, the TEA present in the system may have probably led to the formation of vinyl functional groups, which causes the polymerization. This is evidenced from the Fourier transform infrared spectroscopy (FTIR). Study of resulting precursor solution heated at 200 °C before decomposition. The spectrum showed a broad peak in the region from 2900 – 3140 cm^{-1} , which was due to the polymerization through vinyl group formation during the heat treatment of the precursor solution. This confirms that the polymerization has occurred during the heat. The water-soluble metal ions/metal coordinated complexes become uniformly

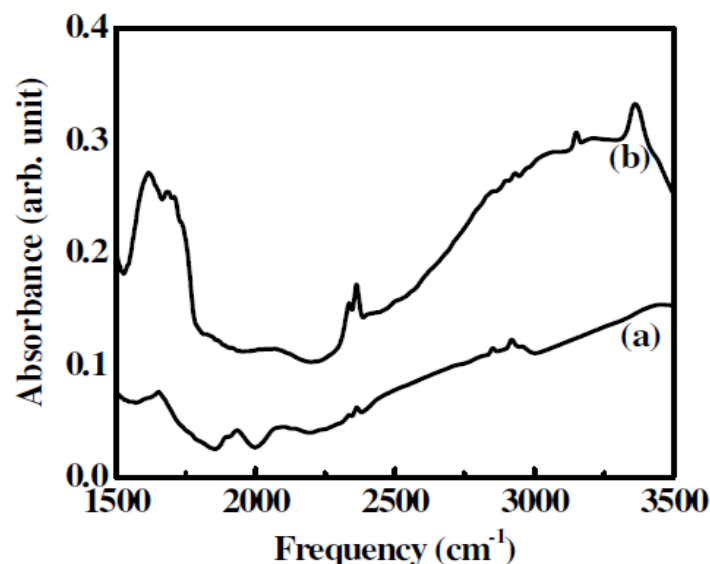


Fig.1.2. FTIR spectra of (a) TEA (Triethanol amine) without heat treatment and (b) Solution of TEA complexed with metal ion just before decomposition.

anchored in the generated polymeric network structure and this possibly serves to prevent their segregation or any intermittent precipitation from the homogeneous precursor solution during evaporation. Complete evaporation of the precursor solution resulted in a highly branched polymeric structure, with the metal ions homogeneously lodged in its matrix. The polymeric structure probably serves as a template for the generation of a voluminous matrix of a polar mesoporous carbon-rich precursor mass on oxidation. This nitrogen atom-enriched precursor mass of mesoporous carbon may have favored the accommodation of the metal ions/metal ion complexes in its matrix. Slow volatilization of this mesoporous carbonaceous residue in the precursors, through low-temperature calcination in dynamic air oxidation provided the condition for the synthesis of the nanoparticles of the respective mixed-oxide systems treatment of TEA complexes with metal ions.

2.2 Characterization

2.1.1 X-ray diffraction measurements

Samples have been characterized by XRD patterns at room temperature using Philips PW1710 X-ray Diffractometer, equipped with a vertical goniometer and CuK_α radiation source of wavelength ($\lambda = 1.54 \text{ \AA}$). XRD patterns for both nanocrystalline and bulk samples are shown in Fig. 2.3. In this figure we have marked the major peaks in the diffraction pattern. The observed values of the diffraction angles (2θ) (nanocrystalline and bulk) match quite well with the standard JCPDS file (86-1326) of Y_2O_3 and the patterns exhibit cubic symmetry (space group $\text{Ia}\bar{3}$).

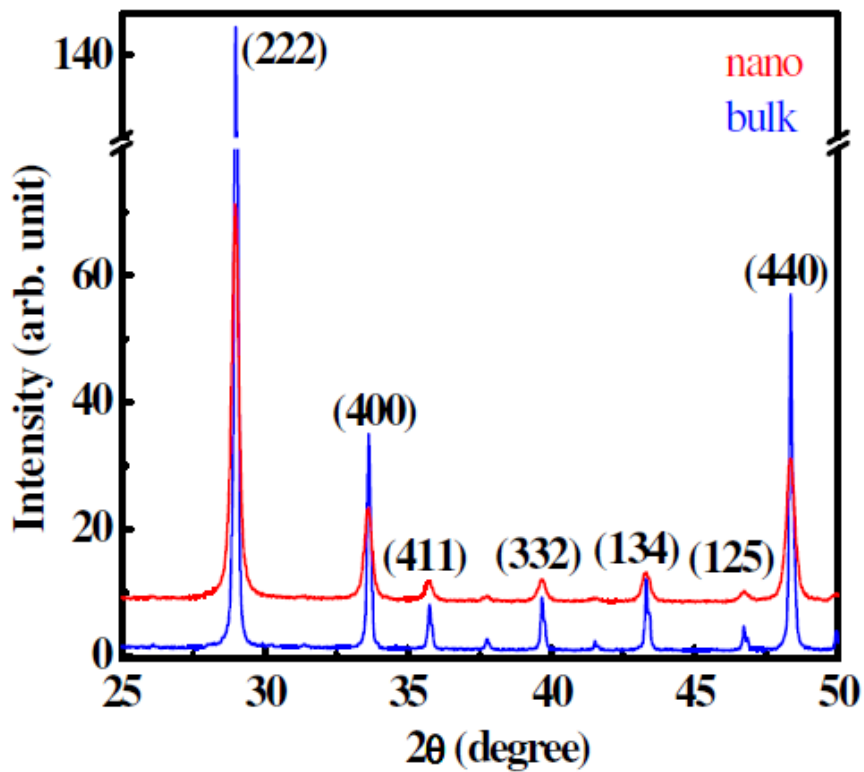


Fig. 1.3. XRD pattern for nanocrystalline and bulk phosphor

2.1.2 Transmission electron microscopy measurements

Samples for TEM are deposited onto 300 mesh copper TEM grids coated with 50 nm carbon films. Nanocrystalline samples, dissolved in acetone, are placed on the grid drop-wise. The excess liquid is allowed to evaporate in air. The grids are examined in JEOL 2010 microscope with Ultra-High Resolution (UHR) pole-piece using a LaB₆ filament operated at 200 kV. TEM image of nanocrystalline Y₂O₃:Eu³⁺ are shown in Fig 2.4.(a). The frequency plot of the size distribution, shown in Fig. 2.4.(b), is obtained by measuring the size of ~ 150 particles per sample.

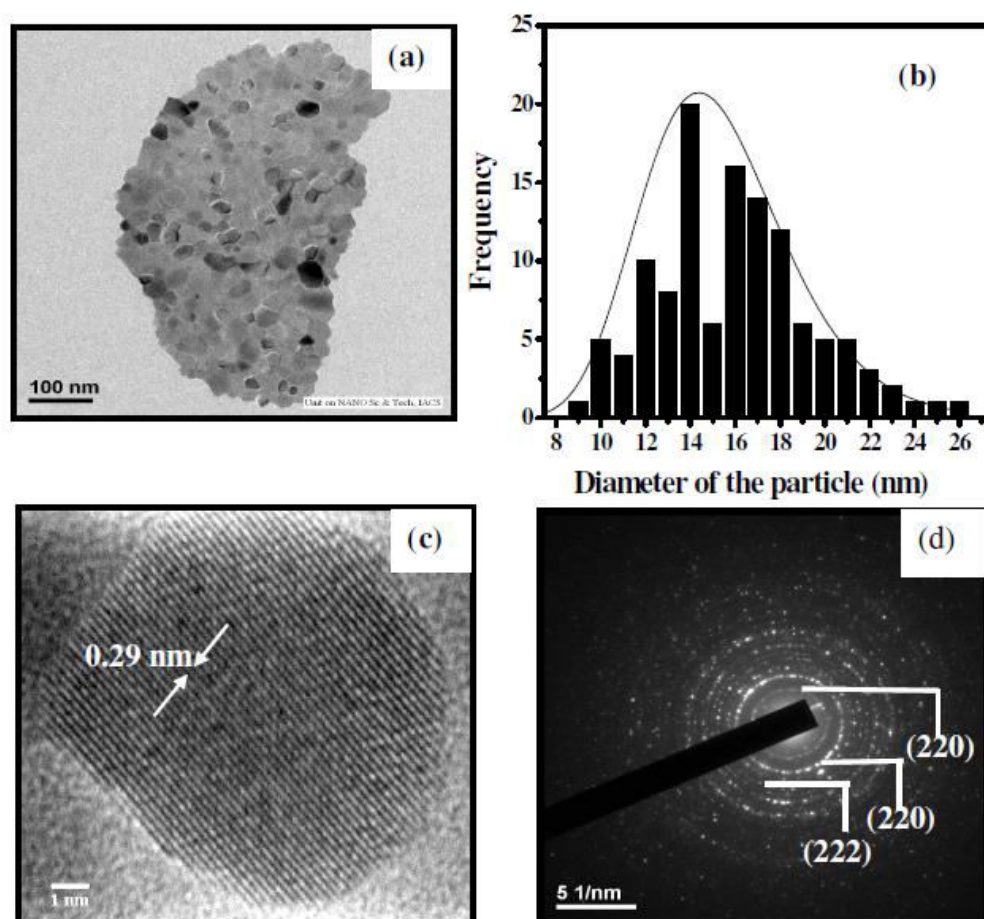


Fig. 1.4. (a) TEM image (b) frequency plot (c) HRTEM image and (d) SAED pattern of

2.1. Photoluminescence Emission Spectra

Luminescence and Raman spectra are obtained using a 1200 g/mm holographic grating, a holographic supernotch filter, and a Peltier cooled CCD detector. We use a 488 nm Argon ion laser of power 30 mW (on the sample-head) as our excitation source. The electronic transition spectra over the range between 490 nm and 900 nm are shown in Fig. 2.5. Many of these transitions sat is for the magnetic dipole selection rules ($\Delta J = 0, \pm 1$ with $J = 0 \Delta J = 0$) in an intermediate coupling scheme [18]. In free Eu^{3+} , the ${}^5\text{D}_0 \rightarrow {}^7\text{F}_2$ transition is forbidden (for both magnetic and electric dipoles). This holds true in a crystalline environment, which has inversion symmetry. It is well established that in the body centered cubic structure of Yttria, Eu^{3+} replaces Y^{3+} in two different sites, 75% of these sites are with C_2 and the other 25% are with S_6 symmetry. Between these two the former does not have the inversion symmetry [19-23]. According to the theory of Judd [24] and Ofelt [25] the ${}^5\text{D}_0 \rightarrow {}^7\text{F}_2$ transition becomes electric dipole type, due to an admixture of opposite parity $4f^{n-1}5d$ states by an odd parity crystal field component. ${}^5\text{D}_0 \rightarrow {}^7\text{F}_{3,5}$ transitions have a mixed character, magnetic dipole intensity usually to first order and electric dipole intensity to second order [26]. The ${}^5\text{D}_0 \rightarrow {}^7\text{F}_3$ transition exhibits a relatively larger intensity than what is expected because of its large induced electric dipole character. The large oscillator strength of the ${}^5\text{D}_0 \rightarrow {}^7\text{F}_3$ transition may be attributed to significant crystal-field induced mixing of the ${}^7\text{F}_3$ state to ${}^7\text{F}_2$ state, leading to the transfer of energy from ${}^5\text{D}_0 \rightarrow {}^7\text{F}_2$ to ${}^5\text{D}_0 \rightarrow {}^7\text{F}_3$ transition [27]. ${}^5\text{D}_0 \rightarrow {}^7\text{F}_{4,6}$ transitions are electric dipole in character and have appreciable intensities [26]. The magnetic dipole and electric quadrupole allowed transitions are forbidden for $\text{J}_0 \rightarrow \text{J}_0$ line. The theory of Judd and Ofelt does not explain the ${}^5\text{D}_0 \rightarrow {}^7\text{F}_0$ fluorescence of Eu^{3+} ion because the $\text{J}_0 \rightarrow \text{J}_0$ transition is forbidden even in the presence of non-centro-symmetric potential. The origin of this emission line can be explained by the variation in crystal field potential, which causes the mixing of odd parity $\text{J} = 1$ states into the ${}^7\text{F}_0$ and ${}^5\text{D}_0$ states [28]. From the fluorescence line-narrowing experiment, it has been shown that the ${}^5\text{D}_0 \rightarrow {}^7\text{F}_0$ borrows its intensity from ${}^5\text{D}_0 \rightarrow {}^7\text{F}_2$ line through the J-mixing in this material [29]. Other than the above transitions, direct band-to-band transition and excitonic emission are expected to appear at 200 and 211 nm [30] in this system.

We could not study these emission lines due to our experimental limitations (recall that we have used 488 nm as the wavelength of our excitation source). No bands are reported below 490 nm. However, electronic transition from 5D_3 to 7F_2 is known to occur in this region [7].

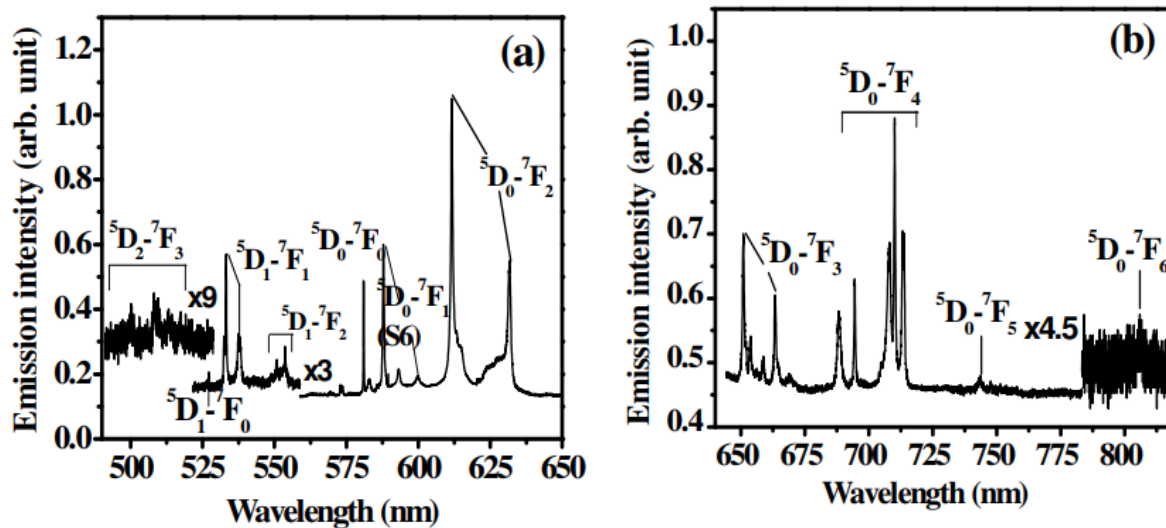


Fig. 1.5. Emission spectrum of nanocrystalline $Y_2O_3:Eu^{3+}$ for $\lambda_{exc} = 488$ nm. Intensities of (a) and (b) are not in the same scale.

In Fig.1.6. We have shown the energy level diagram of the low-lying states of the Eu^{3+} ion in nanocrystalline Y_2O_3 :
 Eu^{3+} , as obtained from our PL measurements.

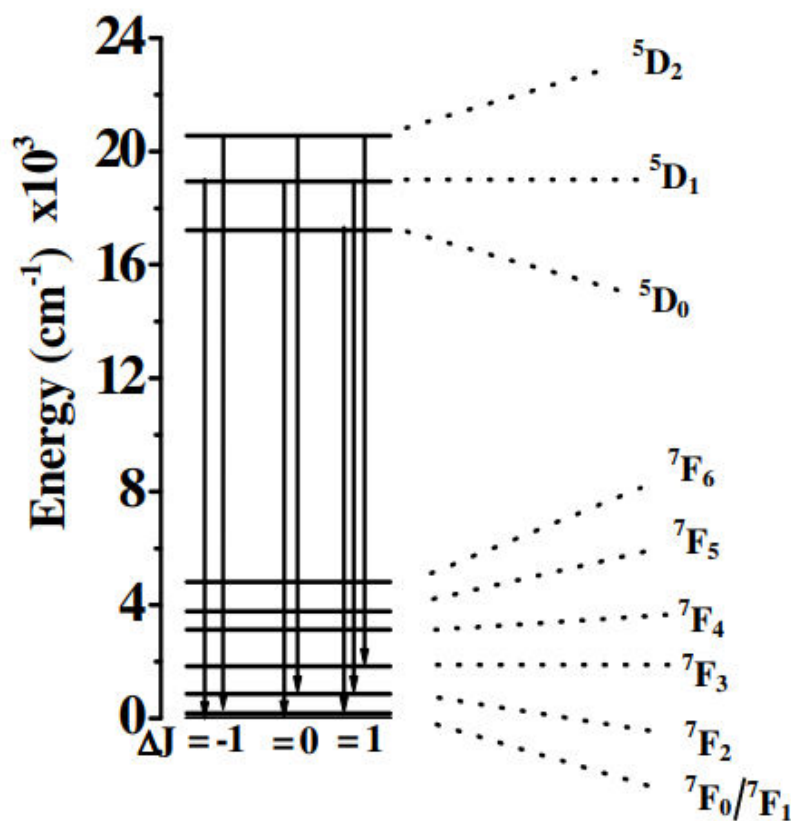


Fig.1.6. Energy level diagram of Eu^{3+} in nanocrystalline $\text{Y}_2\text{O}_3:\text{Eu}^{3+}$

It is well known that a strong energy transfer takes place from S_6 to C_2 site, which gets stronger with increase in Eu^{3+} content [31]. Consequently, the ratio of the emission intensity of C_2 site to the emission intensity of S_6 site also increases with increase in Eu^{3+} concentration in the sample [28]. Previous emission study on cubic bulk $\text{Y}_2\text{O}_3:\text{Eu}^{3+}$ has shown that only the transitions $^5\text{D}_0 \rightarrow ^7\text{F}_1$ originate from S_6 site [32, 33], whereas nearly all of the other features in the electronic spectrum are due to Eu^{3+} ion in C_2 sites. The different behavior of Eu^{3+} ion in two different lattice sites is due to the large diameter

2.4 Photoluminescence (PL) properties of nanocrystalline and bulk phosphors:

In Fig. 1.8, we have compared the most intense electronic transition line at 612 nm in the spectra for both nanomaterial and the bulk system (both the cases concentration of Eu^{3+} is 4 at wt% w.r.t Y^{3+}). Both the spectra have been fitted with three Lorentzian line shapes. In the non-linear least square fit the peak position, width of the spectral line and its intensity have been kept as varying parameters. As shown in Fig. 2.8., the luminescence intensity of 612 transitions from nanocrystalline sample is slightly less than that observed in bulk sample.

Surface states are the sources of non-radiative recombination centers. Due to high surface to volume ratio in nanoparticles compared to the corresponding bulk material the non-radiative recombination processes dominate in the former. This, in turn, decreases the luminescence efficiency in nanoparticles [35]. Furthermore, there is a possibility of the decrease in luminescence intensity due to absorption process by impurities in nanostructured materials. This, in turn decreases the luminescence efficiency of nanoparticles.

However, here we would like to point out that the drop in intensity in nanocrystalline sample compared to the corresponding bulk material, prepared by us, is much less than what has been reported before in the literature [35]. We note that the appearance of all lines $^5\text{D}_3$, $^5\text{D}_2$, $^5\text{D}_1$, signify absence of too many non-radiative cross-relaxation processes in nanocrystalline sample.

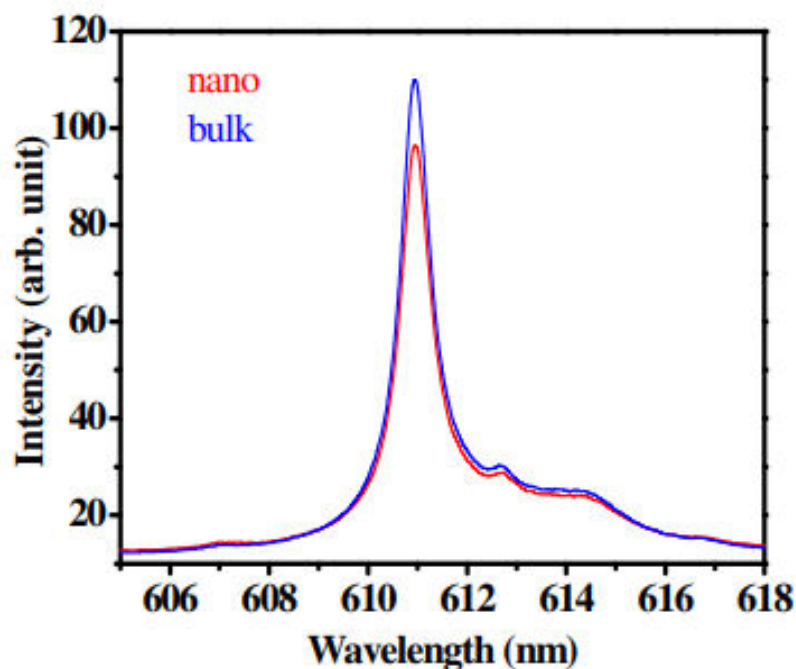


Fig. 1.8 Emission spectrum of 612 nm line for nanocrystalline and bulk phosphors

2.5 Conclusions

In this paper, we have reported optical properties of cubic nanocrystalline rare-earth-doped inorganic oxide, $Y_2O_3:Eu^{3+}$, of average particle size 15 nm. The electronic energy levels of this material are obtained from the PL measurements. The analysis of the variation in intensity of the luminescence spectrum at 612 nm for $Y_2O_3:Eu^{3+}$ as a function of Eu^{3+} concentration in the host lattice reveals that the dopant concentration of 4 at. wt % exhibits maximum intensity of the emission peak for ${}^5D_0 \rightarrow {}^7F_2$ transition beyond “Concentration Quenching” take place.

References

- [1] Brierley M. C. and France P.W., *Electron. Lett.* 23 (1987)815.
- [2] Graeve O. A. and Corral J. O., *Opt. Mater.* 29 (2006)24.
- [3] Rossi P., Brice D. K., Seager C.H., Mcdaniel F.D., Vizkelethy G. and Doyle B.L.,
Nuclear Instruments and methods in Physics Research B, 219-220 {2004}327.
- [4] Blasse G. and Grabmaier B.C., *Luminescent Materials* Springer, Berlin (1994). [5] Ronda C. R., *J. Lumin.* 72 (1997)49.
- [6] Behrens E. G., Durville F.M., Powell R.C. and Blackburn D. H., *Phys. Rev. B* 39 (1989)6076.
- [7] Silver J., Martinez-Rubio M.I., Ireland T.G., Fern G.R. and Withnall R., *J. Phys. Chem. B* 105 (2001) 9107.
- [8] Mishra K.C., Berkowitz J.K., Johnson K.H. and Schmidt P.C., *Phys. Rev. B* 45 (1992)10902.
- [9] Husson E., Proust C., Gillet P. and Itié J.P., *Mater. Res. Bull.* 34 (1999)2085.
- [10] Mitsunaga M. and Uesugi N., *J. Lumin.* 48-49 (1991)459.
- [11] Pappalardo R.G. and Hunt R.B., Jr., *J. Electrochem. Soc.* 132 (1985)721.
- [12] Klassen D.B.M., van Ham R.A. and van Rijn T.G.M., *J. Lumin.* 43 (1989)261.
- [13] Konard A., Almansötter J., Reichardt J., Gahn A., Tidecks R. and Samwer K., *J. Appl. Phys.* 3 (1999)1796.
- [14] Schaik V. W. and Blasse G., *Chem. Mater.* 4 (1992)410.
- [15] Erdei S., Roy R., Harshe G., Juwhari H., Agrawal D., Ainger F. W. and White W. B., *Mater. Res. Bull.* 30 (1995)745.
- [16] Pathak A., Mahapatra S., Mahapatra S., Biswas S., Dhak D., Pramanik N., Taraphder A. and Pramanik P., *Am Ceram. Soc. Bull.* 83 (2004)9301.

- [17] Roy A. and Sood A. K., *Phys. Rev. B* 53 (1996)18.
- [18] Gschneidner K. A. and Eyring L., *Hand-book of Physics and Chemistry of Rare- Earths*, Elsevier, Amsterdam/New York(1979).
- [19] Chang N. C. and Gruber J. B., *J. Chem. Phys.* 41 (1964)3227.
- [20] Silver J., Martinez-Rubio M. I., Ireland T. G. and Withnall R. J., *J. Phys. Chem. B* 106 (2001) 7200.
- [21] Paton M. G. and Maslem E. N., *Acta. Crystallogr.* 19 (1965)307.
- [22] Ishibashi H., Shimomoto K. and Nakahighashi K., *J. Phys. Chem. Solids* 9 (1994) 809.
- [23] Mitric M., Antic B., Balanda M., Rodic D. and Napijalo M. L., *J. Phys. Condensed Mater.* 9 (1997)4103.
- [24] Judd B. R., *Phys. Rev.* 127 (1962) 750.
- [25] Ofelt G. S., *J. Chem. Phys.* 37 (1962) 511.
- [26] Ram S. and Sinha S. K., *J. Solid State Chem.* 66 (1987)225.
- [27] Kirby A. F. and Richardson F. S., *J. Phys. Chem.* 87 (1983) 2557.
- [28] Nieuwpoort W. C. and Blasse G., *Solid State Commun.* 4 (1966)227.
- [29] Nishimura G., Tanaka M., Kurita A. and Kushida T., *J. Lumin.* 48-49(1991)473.
- [30] Tomiki T., Tamashiro J., Tanahara Y., Yamada A., Fukutani H., Miyahara T., Kato H., Shin S. and Ishigame M., *J. Phys. Soc. Jpn.* 55 (1986)4543.
- [31] Buijs M., Meyerink A. and Blasse G., *J. Lumin.* 37 (1987)9.
- [32] Haber J., Hellwege K. H., Kobler K. H., Murmann U., *Z. Phys.* 237(1970)189.
- [33] Forest H. and Ban G., *J. Electrochem. Soc.* 116 (1969)474.
- [34] Tseng Y.-H., Chiou B.-S., Peng C.-C. and Ozawa L., *Thin Solid Films* 330 (1998) 173.

- [35] Schmechel R., Kennedy M., Seggern V. H., Winkler H., Kolbe M., Fischer R. A., Xiaomao Li, Benker A., Winterer M. and Hahn H., *J. Appl. Phys.* 89(2001)1679.